Selective and localized embrittlement of metal by cathodic hydrogenation utilizing electrochemical jet

Yonghua Zhao [a],[*], Chong Zhao [a], Shuai Wang [a], Satoru Kakudo [b], Masanori Kunieda [b]

[a] Department of Mechanical and Energy Engineering, Southern University of Science and Technology, Shenzhen, 518055, China
[b] Department of Precision Engineering, The University of Tokyo, Tokyo, Japan

ARTICLE INFO

ABSTRACT

Electrochemical jet processing (EJP) is an easy-to-implement technology for creating complex microstructures based on anodic dissolution without requiring specially designed cathodes. In this study, a new electrolyte-jet-based surface modification method based on the principle of cathodic hydrogenation, namely, electrochemical jet hydrogenation (EJH), was proposed for the first time to selectively modify the material in aspects of its brittleness. In this method, a workpiece is innovatively set as the cathode, and hydrogen evolution occurs locally on the cathode surface within the jet impinging area, leading to a localized H-treatment of the cathode material. The hydrogen-material interaction can alter the surface material property and result in localized surface modification, for example, material ductile-brittle transition by hydrogen embrittlement (HE). In this research, the proposed method was validated on niobium metal. According to the results, evident localized embrittlement was achieved, and the degree of embrittlement was precisely controlled by adjusting the electrochemical parameters mainly including current density and processing time. As a selective surface modification method, EJH can be applied as an assistive technology in hybrid machining of difficult-to-machine superalloys where localized surface modification of ductile-brittle transition is expected.

1. Introduction

Electrochemical Jet Machining (EJM) [1,2] is an easy-to-implement precision technology that utilizes an electrolyte jet impinging target workpiece to realize selective surface structuring, texturing or finishing based on electrochemical principle. As an adaption of electrochemical machining, EJM needs no tool electrode with a specific shape, and machining is performed by controlling the electric current and the nozzle movement [3,4]. So far great attention has been paid because of its advantages such as micro-scale resolution, no thermal affected zone, residual stress-free smooth surface finish, and high flexibility. By traversing the jet over the workpiece, various complicated patterns can be created without the use of a special mask because of its good localization [5–7]. By controlling the electric charge transport process, the electrochemical finishing of workpiece can be achieved [8]. In addition, EJM can be used not only for removing processes by anodic dissolution but also for the coloring process by anodic oxidation [9]. Furthermore, by reversing the polarity to set the workpiece cathode, selective electroplating [10] and 3D additive manufacturing can be performed [11]. Up to present, however, except for electrochemical jet deposition, there

have been few researches on EJP techniques when the workpiece is cathodic. It is well-known that by setting the workpiece cathode, hydrogen ion in the electrolyte will acquire electrons and evolve on the cathode surface within the jet impinging zone. The reduced hydrogen atoms may interact with workpiece material, e.g., chemically bond with surface material to form a hydride or diffuse into the lattice, resulting in an alteration of surface physical-mechanical properties.

One of the most common results caused by hydrogen-material interaction is hydrogen embrittlement (HE), which is a well-known phenomenon whereby metals lose ductility and become brittle and fracture as a result of the introduction and diffusion of hydrogen into the material [12,13]. Significant work has been undertaken to explore its mechanism to limit the extent, even avoid HE. Martin et al. discussed the universality of HE phenomenon of a range of structural materials including steel, iron, and nickel [14]. Álvarez et al. demonstrated the phenomenon of fracture toughness change of structural steels after HE [15]. Lynch discussed various mechanisms of HE in steel and the phenomena supporting them, such as hydride formation and adsorption-induced dislocation-emission [16]. In electrochemical machining of niobium using a flat jet with bipolar pulses conducted by
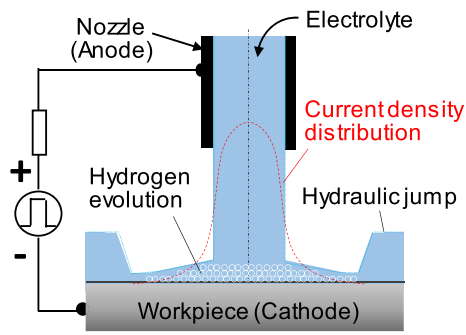
Fig. 1. Principle of the electrochemical jet hydrogenation.

Kakudo et al., the deformation and embrittlement of the machined area was confirmed, which was thought to be caused by hydrogen [17,18]. Despite the variety and complexity of HE mechanism, the introduction of hydrogen to the material surface and the association and movement of hydrogen with material dislocations are comprehended as the principal causes leading to premature failure of material [12,13].

However, it is presumed that if the hydrogen-material interaction (hereafter referred to as hydrogenation) process can be precisely localized and controlled, selective surface modification, e.g. local ductile-brittle transition of material [19], can be realized, which has high potential to improve the machinability of superalloy material to a considerable extent. Superalloys such as titanium and nickel-based alloy are well-known difficult-to-machine materials due to their high tensile strength, low thermal conductivity, and high adhesion. In mechanical machining of superalloys, work hardening and tool wear are notable, which significantly deteriorates the machining performance [20]. On the other hand, it has been reported that the machinability of difficult-to-machine superalloy materials can be improved by appropriate modification of the material ductile-brittle property by hydrogen embrittlement [21]. Specifically, an increase of the material brittleness can decrease the machining force by reduction of material fracture strength and reduce the tool temperature, thus leading to longer tool life and an improved machining performance. Based on the application background discussed above, this work proposed a novel method of electrochemical jet hydrogenation (EJH) for localized material surface modification by utilizing the HE phenomenon.
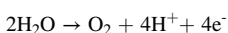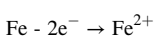
2. Principle of electrochemical jet hydrogenation (EJH)

Electrochemical jet hydrogenation (EJH) employs a similar experimental system as that in electrolyte jet machining (EJM). As shown in Fig. 1, EJH is carried out by jetting electrolytic aqueous solution from a nozzle toward the workpiece while applying a voltage to the gap. However, instead of the anode, the workpiece is set as the cathodic by attaching it to the negative pole of the power supply. Correspondingly, the jet nozzle was connected to the positive pole. Owing to the potential difference, a current density of Gaussian spatial distribution could be obtained within the jet impinging zone on the workpiece surface, as the red dotted line shown in Fig. 1, which is similar to that in EJM calculated by Yoneda and Kunieda [22]. The electrochemical reactions occurring at the anode and cathode can be expressed as bellows:

Cathode:

$$2H_2O + 2e^- \rightarrow 2OH^- + H_2$$
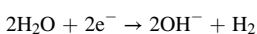
Anode (Stainless 304 jet nozzle):

$$Fe - 2e^- \rightarrow Fe^{2+}$$

$$2H_2O \rightarrow O_2 + 4H^+ + 4e^-$$

Accordingly, hydrogen is evolved on the cathode surface, as illustrated in Fig. 1, and the amount of hydrogen liberation can be calculated
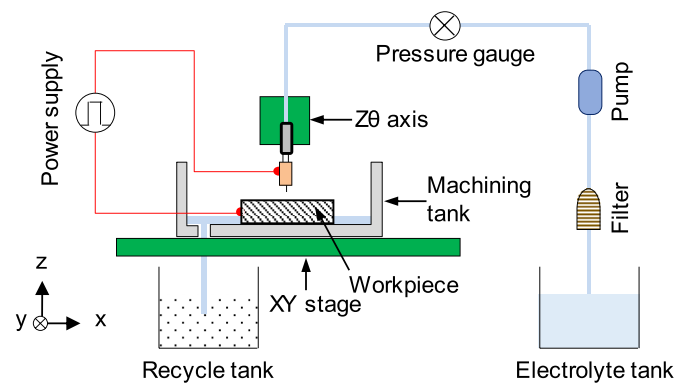

Fig. 2. Experimental setup for electrochemical jet hydrogenation process.

using the current density distribution based on Faraday's law of electrolysis (Eq. (1)) and the ideal gas law (Eq. (2)) as shown below.

$$n = \frac{J}{a*F} \tag{1}$$

$$PV = NRT \tag{2}$$

Where n is the amount of substance liberated at an electrode per unit area per unit time [mol/(m²*s)], J stands for the absolute value of current density [A/m²], a is the valence of the substance, F is Faraday's constant, P, V and T is the local pressure [Pa], gas volume [m³] and temperature [K], N is the amount of substance [mol], and R is the ideal gas constant [J/(mol*K)].

Differentiate time and area on both sides of the ideal gas equation of state gives:

$$Pv = nRT \tag{3}$$

where v is the volume of gas liberated per unit area per unit time.

Based on the density formula $m = \rho V$ where ρ is the density [kg/m³], by bringing Eq. (1) into Eq. (3), the mass flux of hydrogen gas evolved, N_g, can be derived as the following equation:

$$N_g = \frac{\rho JRT}{2FP} [\text{kg/m}^2\text{s}] \tag{4}$$

As can be seen, the mass flux of hydrogen generation is in direct proportion to current density distribution, which enables the parametric control of the process. The resulted hydrogen species either form chemical bonds with surface material or diffuse through material structure at the atomistic level, making the crystal lattice distorted and leading to the alteration of material properties. Most commonly, the hydrogen-material interaction will make the material more brittle, and eventually cause hydrogen embrittlement. Therefore, it is considered that by EJH, a localized hydrogen modified zone, determined by current density distribution, can be obtained on a workpiece surface with altered physical-mechanical properties. Furthermore, by traversing the jet over the workpiece, selective surface modification can be achieved.

3. Experimental method and material

Experiments were carried out using a home-made CNC platform, as shown in Fig. 2. A numerically controlled 4-axis positioning system was employed to realize the relative movement between the nozzle and workpiece, with the workpiece placed on the XY stage and the nozzle on the Z-axis. A constant current (CC) power source was employed to supply current between the nozzle and workpiece. The workpiece was connected to the negative pole of the power source while the nozzle served as the anode during the process. The electrolyte was transported to the nozzle and ejected towards the workpiece by an electrolyte circulation system.
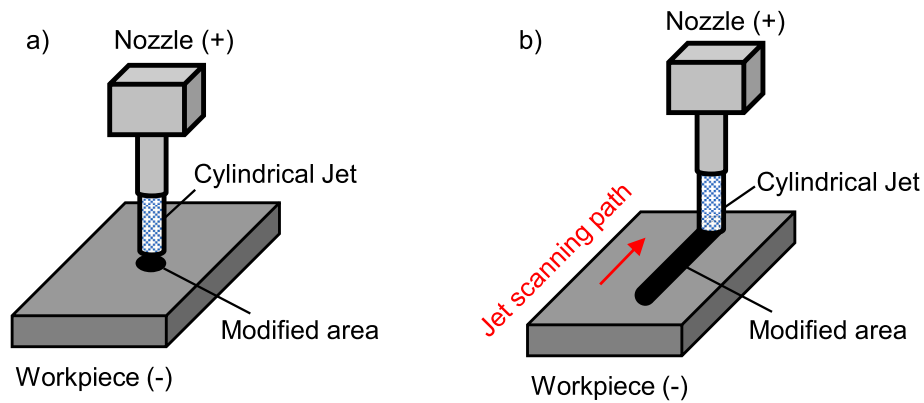
Fig. 3. Processing modes: a) Point processing by keeping the jet still and b) Pattern processing by translating the jet over the workpiece.

Table 1
Experimental conditions for surface modification by EJH.

Jet Diameter	1.11 mm
Nozzle Material	Stainless steel 304
Workpiece	Pure niobium (Nb) plate
Initial gap distance	0.5 mm
Electrolyte	20 wt% $NaNO_3$ (aq.)
Electrolyte flow rate	6 mL/s
Power Supply	Constant Current

Two processing modes, as illustrated in Fig. 3, a) point processing by keeping the jet still and b) pattern processing by translating the jet along the arbitrary path were carried out and the influence of processing modes was discussed in detail in the following parts.

Considering the easiness of low-temperature hydrogen embrittlement [23,24], a niobium metal sheet with a dimension of 30 mm × 10 mm × 0.1 mm was selected as the workpiece to facilitate the experiment. The other experimental conditions are as shown in Table 1. Before and after the experiments, the workpiece was degreased by sonicating in ethanol for 10 min at room temperature, rinsed with deionized water and dried in the air. The surface morphology of the processed workpiece was observed using a scanning electron microscope (SEM, Hitachi TM4000Plus and ZEISS Merlin). The surface profile was examined with a laser scanning confocal microscope (LSCM, Keyence VK-X1000). The change in surface hardness of the processed material was measured using a nanoindentation tester (Hysitron TI-950).

4. Analysis of hydrogen embrittlement region

4.1. Micrographic morphology of HE region

Fig. 4 shows a typical SEM image of the micrographic morphology of the EJH treated surface. The initial surface is also shown for comparison. A clear circular HE region filled with numerous microcracks can be
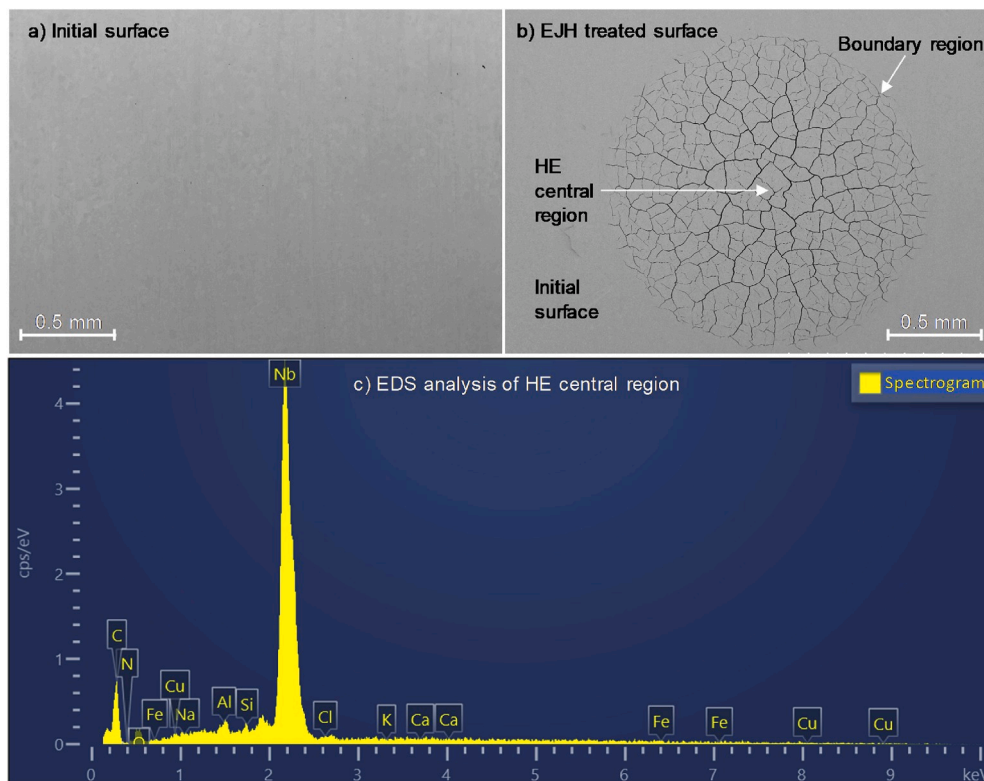

Fig. 4. a) Initial surface, b) Modified surface topography resulted from EJH and c) Elemental analysis for EJH treated surface (Processing time: 60 s, current: 0.6 A).
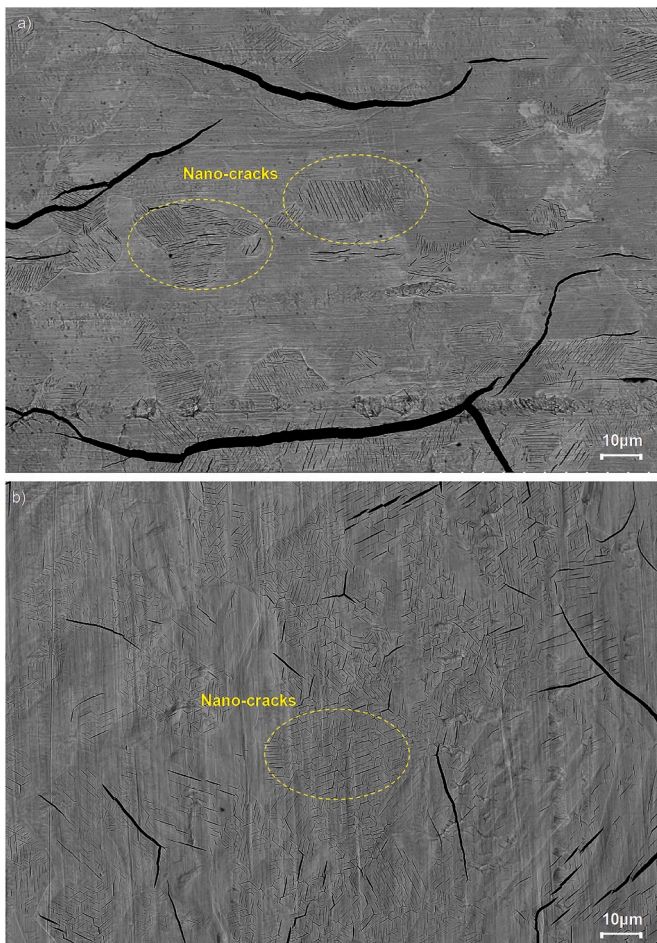
Fig. 5. Formation of regularly distributed nano-cracks in the HE region.

confirmed. The size of the HE region varies with process conditions and will be discussed later. In comparison, the peripheral region presented no visible change. The HE region can be divided into the central area where cracks are clearer with larger crack widths and the boundary area where cracks are smaller and less vivid. Specifically, the width of microcracks around the center was about 10 μm, while the width of most cracks in the boundary area was less than 1 μm. The differences of crack widths between the two areas reveal the disparities of HE degree which are following the normal distribution of the current density on the surface. According to the literature [23,24], hydrogen is relatively innocuous when present in solid solution at low concentration and that hydrogen embrittlement of Nb occurs when it precipitates as a hydride due to the presence of stress. In EJH, it is considered that evolved hydrogen at the cathodic workpiece diffuses through the crystalline structure into the materials and forms hydride along grain boundary or specific crystalline plane [25,26]. Niobium hydride has a much larger volume than the pure Nb and can induce large internal stress in the substrate [25], which consequently leads to hydride embrittlement and forms many cracks in the jet impinging zone. In the peripheral region, however, as the hydrogen concentration in the material is low, no embrittlement occurs. Besides, it was found that the angles of $90°$ and $120°$ between two intersecting microcracks appeared frequently, implying that the microcracks were initiated along either the grain boundary or specific crystal planes of the Nb material. On the other hand, as a cathodic process, there is a possibility of material deposition on the resulted surface during the EJH. Therefore, energy-dispersive X-ray spectroscopy (EDS) analysis for the EJH treated surface is carried out as shown in Fig. 4c. According to the spectrogram, no obvious deposition of material is confirmed under the present conditions except

for a small carbon peak.

The enlarged view of the HE central area in Fig. 5 reveals that in addition to the microcracks with a width of around several microns or larger, nano-scale cracks with a width less than 100 nm distributed among the micro-scale cracks. Furthermore, unlike the microcracks, nano-cracks distributed in the HE region much more concentratedly and presented high regularity. As Fig. 5 shows, a large number of nano-cracks appeared close to one another in a very small area of several tens of square microns which fell in the range of grain size of metal. The boundary of the nano-cracks concentration region, as Fig. 5 a) shows, was quite clear. In addition, nano cracks have arranged either parallel to each other or with an intersection angle of $120°$. It was inferred that the well-arranged distribution pattern of nano-cracks grew along specific crystal direction in Body-Centered Cubic (BCC) system, for instance, $<110>$ direction on the $\{111\}$ plane.

4.2. Geometric change of EJH region

Laser scanning confocal microscopy (LSCM) was employed to study the geometric change of the processed surface. Fig. 6 a) shows an example of the three-dimensional profile of the EJH processed region measured by LSCM. The treated region near the boundary presents a low height profile (blue area) and seems to be removed. However, according to the cross-sectional profile through the center of the EJH zones shown in Fig. 6 b), it is found that the specimen is not removed but locally deformed with an evident curvature by EJH, resulting in a convexity with a height of several tens micrometers at the EJH spot on the workpiece surface. This is consistent with the bending phenomena of Nb film subjected to EJM observed by Kakudo et al. [17,18]. Besides, the height profile at the central area is higher than the peripheral area, which accords with the Gaussian-type current density distribution. The high-frequency components of the profile curve implied the influence of cracks on the overall surface morphology. The profiles of the EJH region under different conditions measured with a Surface Profiler (SURFCOM NEX 031 DX-12, Accretech) are shown in Fig. 6c) and d). It can be observed that almost all of the EJH treated regions are hump-shaped, with the central area higher than the boundary. With longer process time and larger current density, the deformation became more significant with a higher hump-shaped profile, suggesting that the degree of the bulge reflects the degree of HE.

In EJH, the hydrogen atom absorbed on the workpiece surface and diffused through the material or accumulated in voids. The formation of hump can be explained by either the formation of a hydride or the hydrogen molecule near the surface region. On the one hand, the formation of hydride could expand the local volume and generate compressive stress which causes a yield of the material in the tangential direction and bumping in the direction normal to the surface during machining. On the other hand, the recombination of a diffused hydrogen atom at voids or other defects of lattice in the vicinity of the surface could also cause excessive internal hydrogen pressure and induce the local deformation, which is so-called hydrogen-induced blistering [27]. However, in this study, no blistering feature was seen in the SEM images. Therefore, it is highly possible that the hump is formed by the generation of hydride, and the reaction of hydride formation is strongly dependent on the local current density. In the peripheral area, less hydrogen gas was formed due to the lower current density, resulting in a smaller deformation compared to the central zone.

4.3. Thickness of the modified layer

To investigate the modified layer thickness after EJH, the cross-section of the processed surface was observed by SEM. To do this, the EJH processed area was first cut by wire electrical discharge machining (WEDM) to expose the cross-section. Then the section was subjected to a lapping process to eliminate the influence of the WEDM process. The observation result is shown in Fig. 7. It can be seen that the EJH process
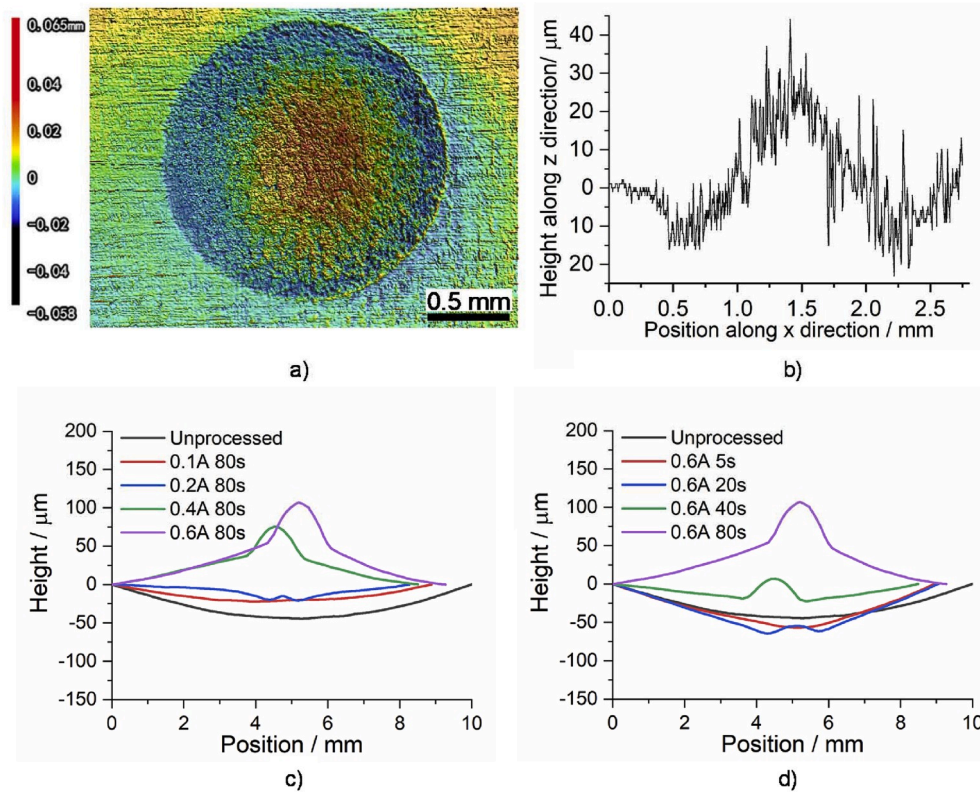
Fig. 6. Surface profile after EJH treatment showing localized deformation at the EJH spot.
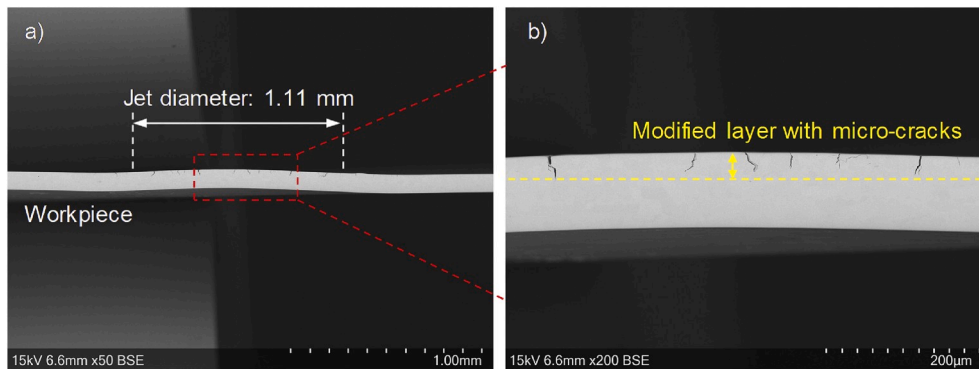

Fig. 7. Cross-sectional observation of EJH processed region showing a modified layer with micro-cracks. (Processing time: 65s, current: 0.6 A).
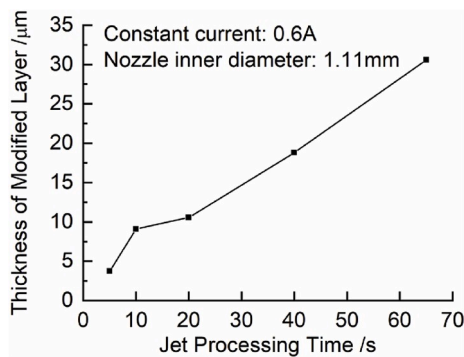

Fig. 8. Variation of EJH modified layer thickness with the processing time.

resulted in a clear modified layer on the workpiece surface with many micro-cracks in it. The size of micro-cracks in the central area was larger than the boundary area, indicating a more significant influence of EJH at the jet center. Furthermore, the cracks propagated not only within the surface but also in the direction perpendicular to the surface. However, nano-scale cracks were difficult to be observed on the cross-sections. If the cracked region was defined as the modified layer, the thickness of the modified layer versus processing time is plotted in Fig. 8. The modified layer thickness was from a few microns to dozens of microns range and with prolonged treatment time it showed a linear increase, indicating that the modified layer thickness can be parametrically controlled.

4.4. Change in hardness of EJH processed surface

As hydrogen atoms are absorbed to the material surface or diffuse into the material during EJH, it is considered that the micro- and
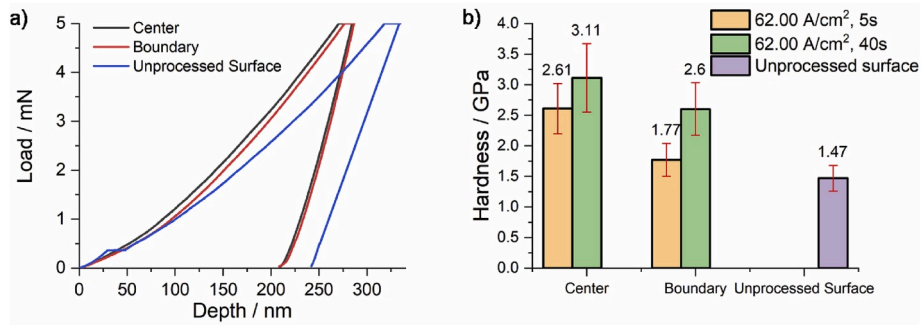
Fig. 9. Change in micromechanical properties of EJH treated surface measured by nanoindentation test: a) Load-displacement curve and b) Hardness of different regions.
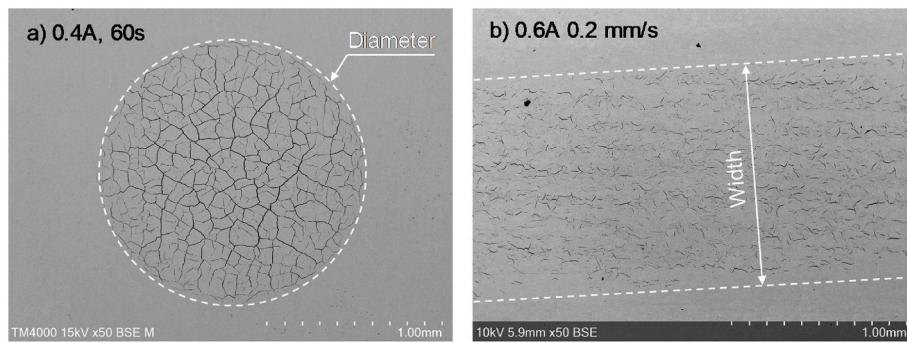

Fig. 10. Evaluation of HE degree in EJH processed area by spot diameter and line width respectively.

nanomechanical properties of the material surface layer also change within the EJH processed region. In the experiments, the micro-hardness measurement of the EJH region was performed by using nano-indentation. Fig. 9 a) shows a comparison of the load-displacement curve involved in the nanoindentation between surfaces with and without undergoing the EJH process. The unloading curve of the EJH region presents a sharper slope than that of the unprocessed surface, indicating that Young's modulus of the material after EJH becomes larger, which accords with the phenomenon that metal material becomes harder after HE takes place [23,24]. Also, the residual displacement becomes smaller, from which it can be presumed that the processed material becomes less plastic and more brittle. Fig. 9 b) shows the results of the indentation hardness calculated from the load-displacement curves using the Oliver-Pharr method [28]. Comparing the material hardness of three regions illustrated in Fig. 5, EJH center area showed the highest microhardness, followed by the boundary region and the unprocessed surface. It is considered that the center area with larger current density has a higher degree of HE, resulting in an improvement of material surface hardness.

5. Evaluation of HE degree in EJH influenced region

As Fig. 10 shows, still jet can result in a circular modified region while translating the jet can realize an arbitrary line pattern of modified surface. In this research, the diameter of the circle and the width of the line resulted from EJH were employed to characterize the HE degree of the EJH influenced area for point processing and pattern processing, respectively.

Furthermore, the area percentage of cracks, which was defined as the proportion of the crack area to the whole area of HE region, was introduced as a criterion to more accurately evaluate the embrittlement degree. As Fig. 11 shows, the crack area has much darker contrast than other areas in the obtained SEM image. With the help of a pixel test program, the brightness of each pixel in the SEM picture was acquired. Through setting a threshold brightness value, dark pixels, which were considered as crack area, could be picked out. The area percentage of cracks in the EJH region could thus be calculated given the dark pixel number and the total number of pixels. This area percentage of crack can describe the density of the cracks.
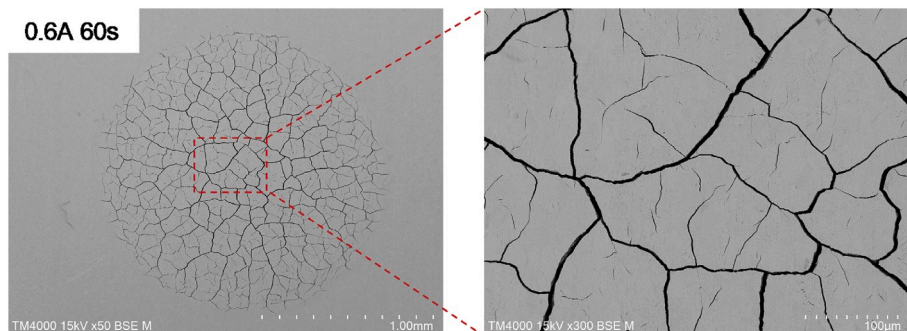

Fig. 11. Calculation of area percentage of cracks in EJH region by image processing technique based on the phenomenon that crack area presents a lower brightness.
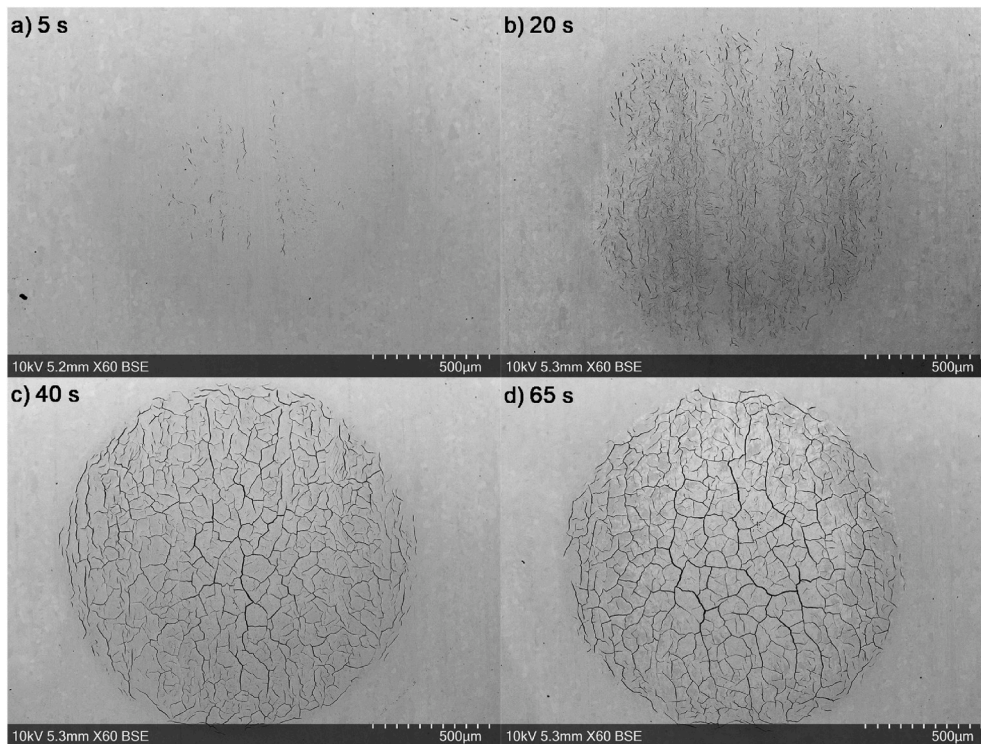
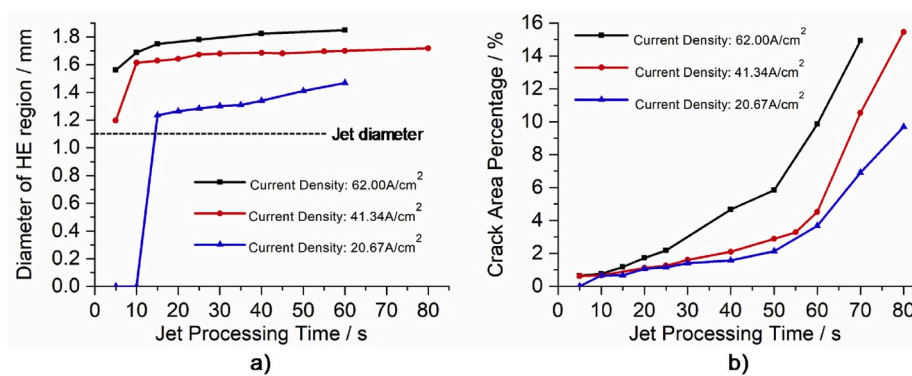**Fig. 12.** Modified surface topography resulted from EJH with different processing time (current: 0.4 A).

Fig. 13. Influence of processing time on EJH zone: a) diameter of EJH zone and b) area percentage of cracks.

6. Optimization of processing parameters

With the aim of a comprehensive understanding of the EJH process,

Fig. 14. Influence of jet translating speed on hydrogenation degree.

various processing parameters were analyzed and the optimization of the EJH process was performed.

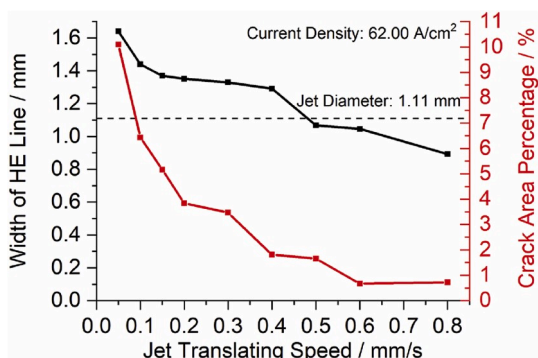### 6.1. Influence of processing time and jet translating speed

Fig. 12 shows the variation of EJH resulted surface with different processing times. It can be seen that in the first few seconds, there were only a very small number of cracks appearing around the center. With increasing the processing time, new cracks were grown and the HE region expanded accordingly with time until it was stabilized. Eventually, the HE region size exceeded the jet diameter, and numerous micro/nano cracks could be observed. In addition, with prolonged processing time, cracks continued to grow longer and wider and meet with each other, resulting in a larger density of cracks. Fig. 13 a) shows the variation of HE region size with time under different current densities. The same mechanism was confirmed when the current density was increased. Furthermore, larger current density could result in a larger diameter of HE region in a relatively shorter time. Fig. 13 b) shows the plot of crack area percentage verse time. It is noticed that the crack density grows
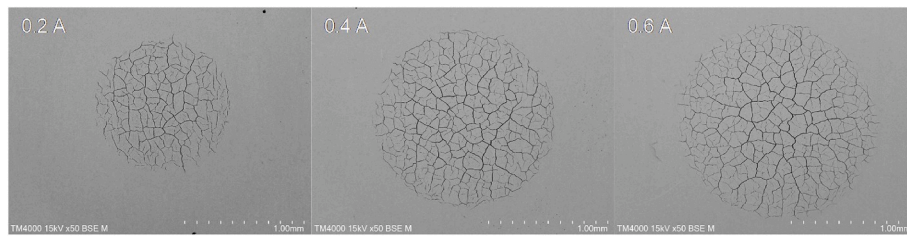
Fig. 15. Change of EJH zone of influence with varying jet current (Jet diameter: 1.11 mm, processing time: 60 s).
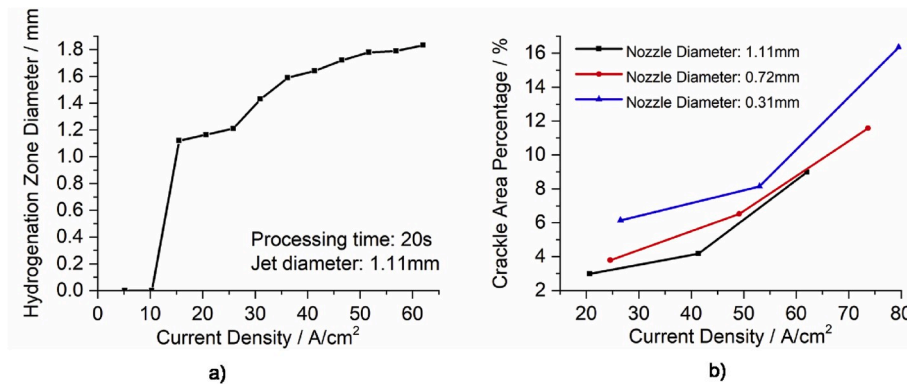

Fig. 16. Influence of current density on EJH in point processing: a) diameter of EJH affected zone and b) crack area percentage (Processing time: 20 s).

with increasing the processing time, although the HE region size becomes constant. In addition, the growth rate is larger in the end than the beginning. It is presumed that the crack growth and propagation continuously occurred in the whole processing time, despite the stabilization of HE region size.

Fig. 14 shows the relationship between HE degree and scanning speed in scanning EJH. It can be found that higher scanning speed resulted in a narrower hydrogenation zone and a smaller area percentage of the crack due to the less processing time per unit area. It is also noticed that the width of the HE line was a little smaller than the diameter of HE point resulted from a still jet under any conditions. For example, at the scanning speed of 0.05 mm/s, the nozzle needed 22 s to move over a distance of the jet diameter 1.11 mm. It can be interpreted as that the nozzle stayed beyond the circle area for 22 s. However, the resulted HE line width was smaller than the HE point diameter resulted from stationary EJH when the jet processing time was 20 s. The cause of this phenomenon is presumed that the relative motion between the nozzle and the workpiece will be of help to facilitate the dissipation of hydrogen away from the workpiece surface, resulting in a lower degree of hydrogen embrittlement.

6.2. Influence of current density

A constant current was applied in the EJH process, and the average current density was defined as the total current divided by the cross-section area of the jet. It can represent the power density level which has an enormous influence on the hydrogenation process. As Fig. 15 shows, larger current density resulted in the larger affected area and more cracks, indicating more severe hydrogen embrittlement. At the peripheral region, as the current density is lower due to the Gaussian distribution of the current density, cracks could hardly be observed, indicating that there is a threshold of current density to initiate cracks.

The same regularity was confirmed after repeating the experiments with more different currents. As shown in Fig. 16a) and b), the area of HE region and the crackle density increase while average current density increasing, which proves that current density has a remarkable influence on the speed of the hydrogenation process and the degree of HE as a result.

7. Patterning by EJH

In EJH, by translating the jet over workpiece along a pre-programmed path, arbitrary patterns could be obtained, which can be utilized for selective surface modification in the form of patterning or texturing. As shown in Fig. 17, jet scanning along a straight-line was performed. It was found that by reducing the scanning speed or increasing the number of reciprocations of the jet, a HE region with many more cracks could be obtained. The width of the HE region
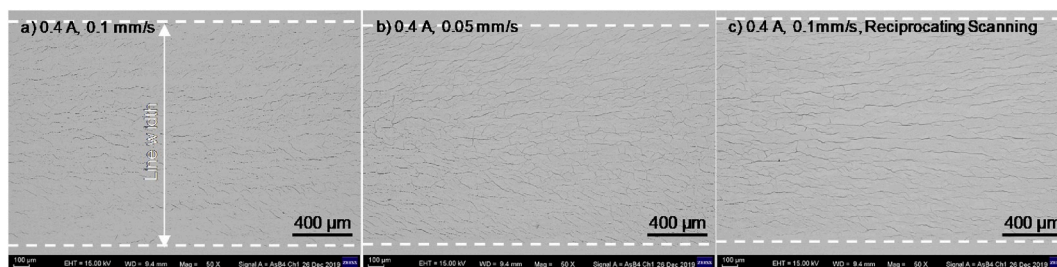

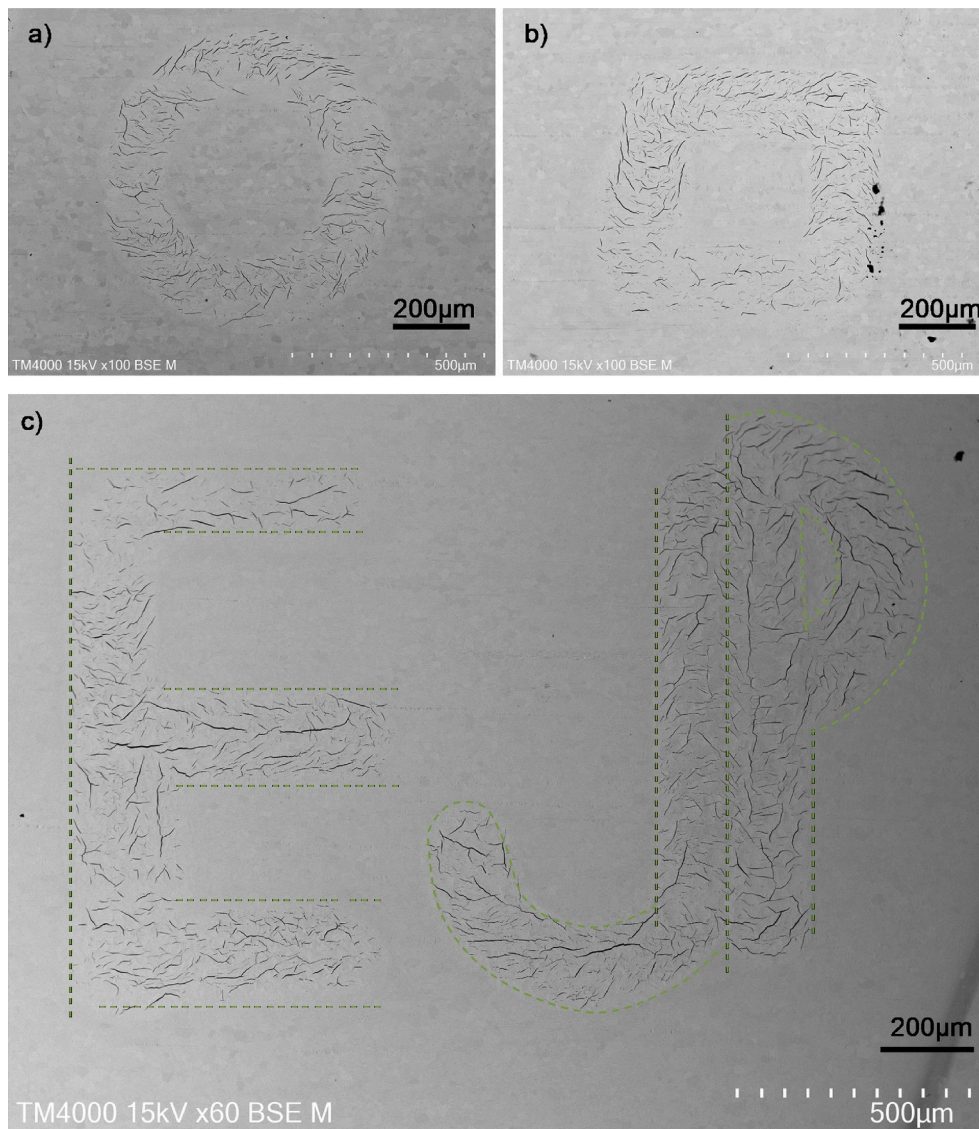**Fig. 17.** Line processing by scanning EJH under different conditions.

Fig. 18. Selective embrittlement of Nb metal by scanning EJH with arbitrary patterns: a) Circle, b) Square, and c) Character EJP (scanning speed: 0.04 mm/s, current: 25 mA, jet diameter: 320 μm).

however increased only at a very limited amount. For instance, at 0.4 A, when the scanning speed is halved or reciprocating scanning was performed, the width of HE lines increased only by less than ten percent and at the same time, much clearer and more cracks could be observed. It is therefore concluded that reciprocating scanning is of help to acquire more localized and concentrated surface modification with higher resolution. Furthermore, by utilizing a micro-scale jet nozzle, micro patterns featuring embrittlement, as shown in Fig. 18, were successfully obtained by scanning EJH.

8. Conclusions

A novel electrochemical jet hydrogenation method to selectively modify material surface taking advantage of cathodic hydrogen evolution was proposed for the first time in this study. The proposed EJH method provides a flexible and efficient but simple means of H-treating of the material with the high locality. In the study, a niobium sample was subjected to EJH and the material embrittlement evidently appeared under cathodic hydrogenation. The embrittled surface showed a micromorphology with a significant number of micro/nano-scale cracks, while the material showed an improved surface hardness and an evident

modified layer. The degree of embrittlement including the crack size and density and the modification layer properties could be parametrically controlled by current density and/or processing time with the electrochemical jet technique. Specifically, the area of HE region increases under increased EJH processing time and current density until it is stabilized at a plateau value. The crack density, however, increased constantly. Larger current density leads to a higher density of cracks. In scanning EJH, with smaller current density, reducing jet scanning speed or increase of the scanning time is of help to acquire more localized and concentrated surface modification with higher resolution. Based on EJH, arbitrary embrittlement patterns with micrometer scale resolution were achieved, verifying the feasibility of this technique. The localized surface embrittlement by EJH is expected to find application in hybrid machining processes which requires a localized ductile-brittle transition to improve the machinability of difficult-to-machine superalloys, e.g., nickel and titanium-based alloys. Other applications of EJH, for example, H-passivation, will be further investigated in the future.

Declaration of competing interest

The authors declare that they have no known competing financial

interests or personal relationships that could have appeared to influence the work reported in this paper.

Acknowledgments

Financial support from the the National Natural Science Foundation of China (NSFC) (No. 51905255), the Shenzhen Science and Technology Innovation Commission (No. JCYJ20190809143217193, No. JCYJ20180504165815601) and the Shenzhen High-level Innovation and Entrepreneurship Fund (No.KQTD20170810110250357) is acknowledged with thanks. The authors are grateful to Ms. Lanxiang Xiao for assistance with the study.

References

[1] Ippolito R, Tornincasa S, Capello G. Electron-jet drilling. Ann CIRP 1981;30(1): 87–9. https://doi.org/10.1016/S0007-8506(07)60901-9.

[2] Kunieda M. Influence of micro indents formed by electro-chemical jet machining on rolling bearing fatigue life. ASME PED 1993;64:693–9.

[3] Kozak J, Rajurkar KP, Balkrishna R. Study of electrochemical jet machining process. J Manuf Sci Eng 1996;118(4):490–8. https://doi.org/10.1115/1.2831058.

[4] Natsu W, Ooshiro S, Kunieda M. Research on generation of three dimensional surface with micro-electrolyte jet machining. CIRP J Manuf Sci Technol 2008;1: 27–34. https://doi.org/10.1016/j.cirpj.2008.06.006.

[5] Hackert M, Meichsner G, Zinecker M, Martin A, Schubert A. Micro machining with continuous electrolytic free jet. Precis Eng 2012;36:612–9. https://doi.org/10.1016/j.precisioneng.2012.05.003.

[6] Clare AT, Speidel A, Mitchell-Smith J, Bisterov I, Murray JW. Surface enhanced micro features using electrochemical jet processing. CIRP Ann 2019;68(Issue 1): 177–80. https://doi.org/10.1016/j.cirp.2019.04.114. 2019.

[7] Natsu W, Ikeda T, Kunieda M. Generating complicated surface with electrolyte jet machining. Precis Eng 2007;31(1):33–9. https://doi.org/10.1016/j.precisioneng.2006.02.004.

[8] Kawanaka T, Kunieda M. Mirror-like finishing by electrolyte jet machining. CIRP Ann - Manuf Technol 2015;64:237–40. https://doi.org/10.1016/j.cirp.2015.04.029.

[9] Mori Y, Kunieda M. Maskless coloring of titanium alloy using electrolyte jet. In: Proceedings of JSEME annual meeting; 1997. p. 13–6 (in Japanese).

[10] Alkire RC, Chen TJ. High-speed selective electroplating with single circular jets. J Electrochem Soc 1982;129(11):2424–32.

[11] Kunieda M, Katoh R, Mori Y. Rapid prototyping by selective electro deposition using electrolyte jet. Ann CIRP 1998;47(1):161–4. https://doi.org/10.1016/S0007-8506(07)62808-X.

[12] Louthan Jr MR, Caskey Jr GR, Donovan JA, Rawl Jr DE. Hydrogen embrittlement of metals. Mater Sci Eng 1972;10:357–68. https://doi.org/10.1016/0025-5416(72)90109-7.

[13] Robertson IM, Sofronis P, Nagao A, Martin ML, Wang S, Gross DW, Nygren KE. Hydrogen embrittlement understood. Metall Mater Trans 2015;46(6):2323–41. https://doi.org/10.1007/s11661-015-2836-1.

[14] Martin ML, Dadfarnia M, Nagao A, Wang S, Sofronis P. Enumeration of the hydrogen-enhanced localized plasticity mechanism for hydrogen embrittlement in structural materials. Acta Mater 2018;165(15 February 2019):734–50. https://doi.org/10.1016/j.actamat.2018.12.014.

[15] Álvarez G, Peral LB, Rodríguez C, García TE, Belzunce FJ. Hydrogen embrittlement of structural steels: effect of the displacement rate on the fracture toughness of high-pressure hydrogen pre-charged samples. Int J Hydrogen Energy 2019;44(29): 15634–43. https://doi.org/10.1016/j.ijhydene.2019.03.279.

[16] Lynch SP. Hydrogen embrittlement (HE) phenomena and mechanisms. In: Stress corrosion cracking. Woodhead Publishing; 2011. p. 90–130. https://doi.org/10.1533/9780857093769.1.90.

[17] Kakudo S, Kunieda M. Surface machining of materials prone to passivation by electrolyte jet scanning. In: Proceedings of the annual meeting of JSEME; 2017. p. 5–8 [In Japanese].

[18] Kakudo S, Kunieda M. Bending of niobium thin plate by electrolyte jet. In: Proceedings of the spring meeting of JSPE; 2018. p. 915–6 [In Japanese].

[19] Song Jun, Curtin WA. Atomic mechanism and prediction of hydrogen embrittlement in iron. Nat Mater 2013;12:145–51. https://doi.org/10.1038/nmat3479.

[20] Kitagawa T, Kubo A, Maekawa b K. Temperature and wear of cutting tools in high-speed machining of Inconel 718 and Ti-6Al-6V-2Sn. Wear 1997;202:142–8. https://doi.org/10.1016/S0043-1648(96)07255-9.

[21] Li S, Wu Y, Wu S. Hydrogen embrittlement enhance ultrasonic assisted grinding of Inconel 718. In: Proceeding of the 22nd international symposium on advances in abrasive technology; 2019.

[22] Yoneda Koji, Kunieda Masanori. Numerical analysis of cross sectional shape of micro-indents formed by the electrochemical jet machining (ECJM). JSEME 1994; 29(62):1–8.

[23] Gahr S, Grossbeck ML, Birnbaum HK. Hydrogen embrittlement of Nb I - macroscopic behavior at low temperatures. Acta Metall February 1977;25(Issue 2): 125–34. https://doi.org/10.1016/0001-6160(77)90116-X.

[24] Grossbeck ML, Birnbaum HK. Low temperature hydrogen embrittlement of niobium II—microscopic observations. Acta Metall February 1977;25(Issue 2): 135–47. https://doi.org/10.1016/0001-6160(77)90117-1.

[25] Schober T, Linke U. A metallographic study of the niobium-hydrogen system Part I. β-phase room temperature morphologies. J Less Common Met 1976;44:63–76. https://doi.org/10.1016/0022-5088(76)90118-1.

[26] Schober T, Linke U. A metallographic study of the niobium-hydrogen system Part II. γ, δ, ζ and ε-phase precipitation. J Less Common Met 1976;44:77–86. https://doi.org/10.1016/0022-5088(76)90119-3.

[27] Myers SM, et al. Hydrogen interactions with defects in crystalline solids. Rev Mod Phys 1992;64:559–617. https://doi.org/10.1103/RevModPhys.64.559.

[28] Cheng YT, Cheng CM. What is indentation hardness? Surf Coating Technol 2000; 133:417–24. https://doi.org/10.1016/S0257-8972(00)00896-3.